ADVANCED FUNCTIONAL MATERIALS
www.afm-journal.de

Lithium Phenolate Complexes with a Pyridine-Containing Polymer for Solution-Processable Electron Injection Layers in PLEDs

Takayuki Chiba, Yong-Jin Pu, Shogo Takahashi, Hisahiro Sasabe, and Junji Kido**

A series of (vinylphenyl)pyridine-based polymer binders, PVPh2Py, PVPh3Py, and PVPh4Py, are designed and synthesized and it is found that mixtures of Liq and the polymers exhibit superior electron injection characteristics as ultrathin (1.6 nm) electron injection layer (EIL) films. They are comparable to those of EILs composed only of Liq. The addition of the polymers does not deteriorate the performance of Liq EILs. Additionally, when the EIL thickness is increased from 1.6 nm to 16 nm, the driving voltages increase and the external quantum efficiencies decrease. The increase in the voltage and decrease in the EQE are suppressed in the device with mixed EILs compared to those observed for the device composed of 100 wt% Liq. Furthermore, the position of the nitrogen in the pyridine ring is considered to influence the electron transport properties of the EILs. The mixing PVPh4Py with Liq improves the driving voltage of the fabricated devices, even with a thick mixed EIL. This reduced dependence of the performance of EILs on their thickness will be advantageous for the coating of large areas using solution processes.

1. Introduction

Polymer light-emitting devices (PLEDs) prepared using a solution process such as spin coating, blade coating, or inkjet printing have the advantages of large area processing and low fabrication costs.[1–4] In the PLEDs, highly reactive low work function metals such as barium and calcium have been widely used in the electron injection layer (EIL) for low operating voltages and high efficiencies.[5–7] However, these metals are unstable in air due to their high reactivity with oxygen and moisture, resulting in the degradation of the device properties. Moreover, the metals are also barely soluble in common organic solvents, and thus cannot be used for solution processing. To realize a solution process for EILs, stable and soluble electron injection materials are required that have solubilities orthogonal to that of the light emitting layer (EML), such that the coating solvent for the EIL dose not dissolve the light emitting layer.[8–11] One approach is to use strongly polarized organic polymers, such as polyelectrolytes, polyethyleneimines, and poly(aminoethylalcohol)s.[12–19] Inserting these polarized polymers between the light-emitting layer and the cathode can result in efficient electron injection. Recently, small molecule electrolytes were also reported to enhance electron injection from the cathode.[20] Another approach involves the use of inorganic salts. Thermal vacuum evaporated films of alkali metal fluorides such as LiF[21] and NaF,[22] are widely utilized as effective EILs for OLEDs. These alkali metal fluorides are not suitable for solution processes due to their low solubility in alcoholic solvents. Conversely, Cs_2CO_3 is relatively soluble in alcohols, can be spin-coated from solution, and has been reported as a solution-processable EIL.[23–25] Cesium stearate is also suitable for the preparation of solution- processing EILs with good electron injection properties and good film formation. In fact, these solution-processed EILs exhibits superior electron injection properties comparable to those of barium and calcium.[26]

We previously reported that solution-processed lithium 8-quinolate (Liq) served as an efficient EIL, and Liq is highly soluble in polar solvents such as alcohols and can be spin-coated onto the light-emitting layer from solution to form films that are resistant to oxidation and less hygroscopic than Cs_2CO_3.[27] In general, the thickness of EILs composed of compounds such as Liq and Cs_2CO_3 must be the ultrathin (<2 nm) to achieve efficient electron injection characteristics due to their poor electron transport properties. However, precise thickness control in the range of a few nanometers is practically impossible for large-scale device using solution processes such as spin coating and blade coating. In this context, only relatively thick EIL films (10–20 nm) can be mass-produced for large PLEDs using solution processing.

Herein, we report the use of a mixture of poly(vinylphenylpyridine) and Liq for solution-processable efficient, thick electron injection layers. Vinyl polymers with high solubilities in alcoholic solvents and good film-forming abilities, such as poly(4-vinylpyridine) (PV4Py) and poly[4-(4-vinylphenyl)pyridine] (PVPh4Py) (**Figure 1**), were used as a binders for Liq, and the effect of the π-conjugation of the polymers on the electron transport and injection characteristics were investigated. The influence of the position of the nitrogen in the pyridine rings was also investigated using poly[2-(4-vinylphenyl)pyridine]

Dr. T. Chiba, Prof. Y.-J. Pu, S. Takahashi,
Prof. H. Sasabe, Prof. J. Kido
Department of Organic Device Engineering
Research Center for Organic Electronics
Yamagata University
4–3–16 Johnan, Yonezawa
Yamagata 992–8510, Japan
E-mail: pu@yz.yamagata-u.ac.jp; kid@yz.yamagata-u.ac.jp

DOI: 10.1002/adfm.201401060

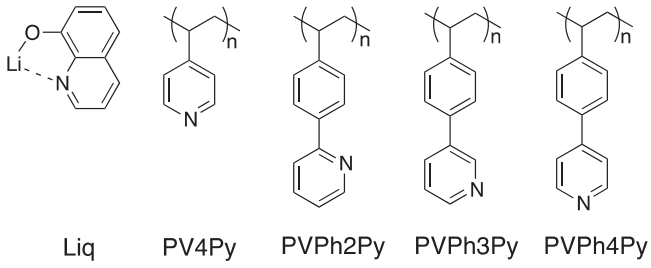

Figure 1. Chemical structures of the compounds.

(PVPh2Py) and poly[3-(4-vinylphenyl)pyridine] (PVPh3Py) (Figure 1). The performance of the EILs prepared from the mixtures of the PVPh4Py and Liq depended on the thickness of the layer (ultrathin layers (approximately 1.6 nm), thin layers (approximately 8.6 nm) and thick layers (approximately 16 nm)) and the type of polypyridine. For devices with ultrathin EIL layers, the performances was not affected by the type of the polymer binder. Conversely, thin and thick layers of PVPh4Py:Liq exhibited higher efficiencies than layer of Liq alone and of Liq with the other polymer binders due to interactions between the Li atoms and the pyridine units of PVPh4Py. These results demonstrated that the conjugation and the nitrogen position of the polypyridine binder mixed with Liq are important for not only enhancing the electron injection property but also reducing the dependence of those properties on the thickness of the EIL.

2. Results and Discussion

2.1. Synthesis and Characterization

The synthetic routes for the three poly(vinylphenylpyridine) (PVPhPy) derivatives are shown in Scheme S1 (Supporting Information). All of the polymers were readily prepared in two steps. The 2-, 3-, and 4- vinylphenylpyridine monomers **1–3** were synthesized via the Suzuki coupling reaction of 4-vinylphenylbromic acid and 2-bromoryridine, 3-bromopyridine, or 4-bromopyridine hydrochloride, respectively. The monomers were polymerized using benzoylperoxide as the radical initiator, and the polymers were obtained in quantitative yield. The detailed synthetic procedures are described in the Supporting Information. The polymers were characterized using elemental analysis, nuclear magnetic resonance (NMR) spectroscopy, and gel permeation chromatography (GPC). The number average molecular weights of PVPh2Py, PVPh3Py, and PVPh4Py were 12 000, 6000, and 40 000, respectively, with molecular weight distributions of 1.9, 2.0, and 2.1, respectively. PV4Py was purchased from Aldrich, and its number average molecular weight and molecular weight distribution were 90 000 and 2.0, respectively. The solubility of the polymers was tested using alcoholic solvents, including methanol, ethanol, 2-propanol, and 2-ethoxyethanol. PV4Py exhibited high solubility in these alcoholic solvents to a concentration of 2 mg mL^{-1}. Conversely, the PVPhPys were slightly less soluble in methanol, ethanol, and 2-propanol, due to the additional phenyl substituent in these compounds. However, 2-ethoxyethanol was a good solvent for the PVPhPys to a concentration of 5 mg mL^{-1}. The position of the nitrogen in the phenylpyridine unit of the polymers did not influence their solubility in alcoholic solvents. These results suggested that 2-ethoxyethanol should be a suitable solvent for the coating of the PVPhPys:Liq mixtures, because most light emitting π-conjugated polymers are not soluble in 2-ethoxyethanol, and thus deposition of an EIL coating on top of the emissive layer should be possible. The thermal properties of the polymers are summarized in **Table 1**. The glass transition temperatures (T_g) were determined via differential scanning calorimetry (DSC). The T_g of PVPh4Py was observed at 185 °C, which is higher than that of PV4Py (146 °C) due to the more rigid structure of the phenylpyridine. The T_g of PVPh4Py was also higher than those of PVPh2Py (162 °C) and PVPh3Ph (140 °C), suggesting that the location of the nitrogen at the 4-position of the PVPh4Py enables stronger intermolecular hydrogen bonding interactions than those in PVPh3Py and PVPh2Py.

In the UV–vis absorption spectra, the PVPhPys exhibited smaller energy gaps (E_g's) than that of PV4Py, because the additional phenyl group participates in extended π-conjugation compared to that possible with only the pyridine group (**Figure 2**). Among the PVPhPys, PVPh2Py exhibited a bathochromically shifted absorption peak compared to those of PVPh3Py and PVPh4Py. The greater π-conjugation of PVPh2Py is probably due to the greater planarity of the structure of 2-phenylpyridine, which results because of the absence of a hydrogen at the ortho position and the consequent reduced steric hindrance. The results of density functional theory (DFT) calculations at the with B3LYP 6–311+G(d,p)//6– 31G(d) level with (4-ethylphenyl)pyridine structures as model molecules, which were obtained using the Gaussian 09 program, supported the higher planarity of PVPh2Py. The dihedral angle of 2-(4-ethylphenyl) pyridine was determined to be 17°, which is smaller than that of 3-(4-ethylphenyl)pyridine (38°) and 4-(4-ethylphenyl)pyridine

Table 1. Physical properties of polymer binders.

Compound	M_n[a)]	M_n/M_w	T_g[e)] [°C]	T_d[f)] [°C]	HOMO[b)] [eV]	E_g[c)] [eV]	LUMO[d)] [eV]
PV4Py	90000	2.0	146	360	6.0	4.4	1.6
PVPh2Py	12000	1.9	162	350	5.8	3.9	1.9
PVPh3Py	6000	2.0	140	340	5.9	4.1	1.8
PVPh4Py	40000	2.1	185	363	6.0	4.1	1.9

[a)]Obtained via gel permeation chromatography (GPC); [b)]Estimated using photoelectron yield spectroscopy (PYS); [c)]Determined from the UV–vis spectra; [d)]Calculated using the highest occupied molecular orbital (HOMO) and energy gap (E_g); [e)]Determined via differential scanning calorimetry (DSC); [f)]Obtained from the thermogravimetric analysis (TGA).

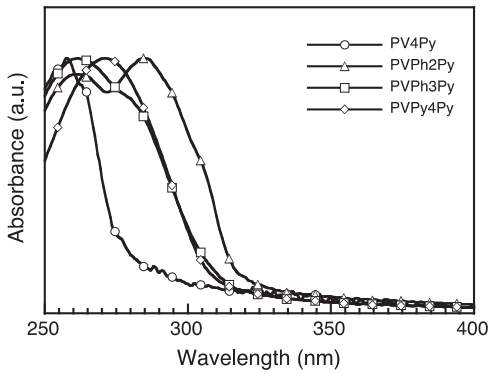

Figure 2. UV–vis absorption spectra of the polymer binder films.

(35°). The highest occupied molecular orbital (HOMO) levels of the polymers were estimated from the ionization potentials determined via photoelectron yield spectroscopy (PYS) to be 6.0 eV for PV4Py, 5.8 eV for PVPh2Py, 5.9 eV for PVPh3Py, and 6.0 eV for PVPh4Py. The lowest unoccupied molecular orbital (LUMO) levels were estimated from the difference in the E_g and the HOMO level to be 1.6 eV for PV4Py, 1.9 eV for PVPh2Py, 1.8 eV for PVPh3Py, and 1.9 eV for PVPh4Py.

2.2. Concentration Dependence of Liq in Ultrathin Layers

Solution-processed multilayer PLEDs were fabricated using the yellow fluorescent polymer poly(9, 9-dioctylfluorene-*alt*-benzothiadiazole) (F8BT) as the EMLs and the polypyridines with Liq for the EILs. F8BT is not soluble in 2-ethoxyethanol, and thus the polypyridines with Liq could be spin-coated on the F8BT layers from 2-ethoxyethanol solutions. The EIL solutions were prepared at concentrations of 1 and 3 mg mL^{-1} in 2-ethoxyethanol for the ultrathin layers (approximately 1.6 nm) and the thin layers (approximately 8.6 nm) and thick layers (approximately 16 nm), respectively, and deposited using different spin speeds. The PLEDs were fabricated with the following configuration: ITO (130 nm)/PEDOT:PSS (30 nm)/poly(9, 9-dioctylfluorene-co-N-(4-butylphenyl)-diphenylamine) TFB (20 nm)/F8BT (80 nm)/polypyridine: Liq/Al (100 nm). The thickness was determined using X-ray refraction analysis for the ultrathin (<10 nm) layers and using a Dektak surface profiler for the thick layers (>10 nm). TFB was used as not only an electron blocking layer due to its shallow LUMO level of 2.6 eV but also as an exciton blocking layer from the direct quenching by PEDOT:PSS. Detailed PLED fabrication procedures are described in the experimental section.

First, the influence of the concentration of Liq in a PVPh4Py:Liq mixture in the performance of the ultrathin layers of around approximately 1.6 nm was investigated. In addition to devices prepared with EIL layers composed of PVPh4Py with 10, 30, 50, or 70 wt%, two control devices were fabricated using ultrathin layers of only Liq and PVPh4Py. The observed electroluminescence of various devices was identical to the emission from F8BT, and no emission was observed from TFB or Liq (Figure S1, Supporting Information). This result indicated that the holes and the electrons were confined within the F8BT and that the recombination of the charges occurred only in the F8BT. **Figure 3**a–c shows the current density–voltage (J–V), luminance–voltage (L–V), and the external quantum efficiency–current density (EQE–J) characteristics of the devices. The device with 100 wt% PVPh4Py exhibited a high turn-on driving voltage of 3.0 V and driving voltages of 5.6 and 8.4 V at 100 and 1000 cd m^{-2}, respectively. The EQE of 0.6% observed

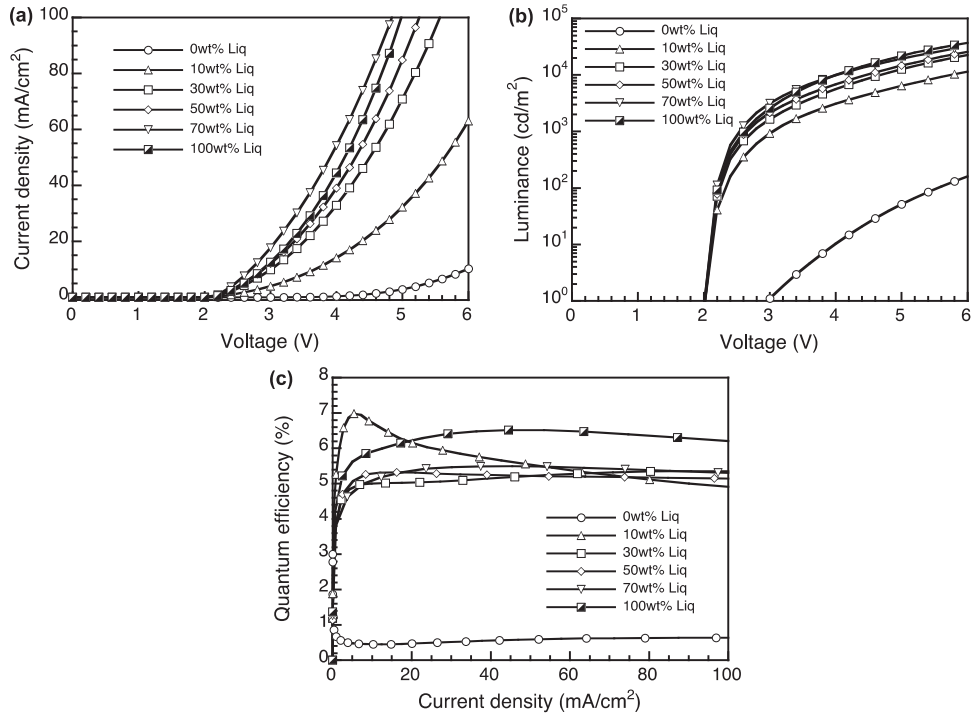

Figure 3. PLED performance with an ultrathin layer of Liq and PVPh4Py at various Liq doping concentrations: a) current density–voltage characteristics, b) luminance–voltage characteristics, and c) external quantum efficiency–current density characteristics.

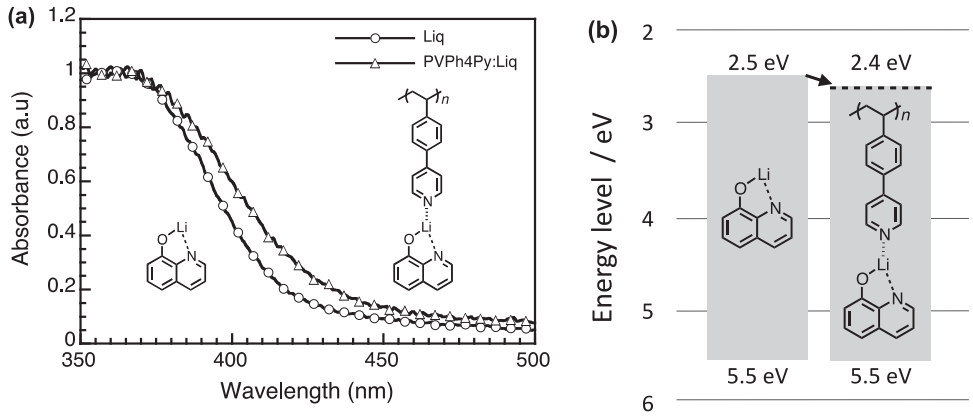

Figure 4. a) UV–vis absorption spectra films of Liq alone and Liq with PVPh4Py film and b) energy levels of the Liq film and PVPh4Py:Liq films.

at 1000 cd m^{-2} for the devices with the 100 wt% PVPh4Py layer were lower than those of the device with PVPh4Py doped with Liq. This result suggested that PVPh4Py itself has poor electron injection property due to its shallow LUMO level of 1.9 eV. However, the device performance dramatically improved when Liq was added to the PVPh4Py. The driving voltage of the devices with PVPh4Py:Liq decreased with increasing Liq concentration from 10 to 70 wt% due to increased electron injection into the F8BT from the Al cathode. The external quantum efficiencies were 4.9–6.9%. These driving voltages and efficiencies were nearly equivalent to those of the device with the ultrathin EIL layer composed of 100 wt% Liq. All of the device characteristics are summarized in Table S1 (Supporting Information). In the device with 10 wt% Liq, balanced charge ratio resulted in the highest power efficiency of 23 lm W^{-1} and an EQE of 6.9% at 1000 cd m^{-2}. Notably, this power efficiency is the highest value reported in the literatures to date for devices with F8BT as the EML.[28] These results indicate that while PVPh4Py itself is not effective as an EIL, mixing it with Liq does not deteriorate the electron-injection properties of Liq and improves the driving voltages and efficiencies of the devices. **Figure 4**a shows that the UV absorption edge of the film prepared from the mixture of Liq and PVPh4Py with 50 wt% Liq was red shifted by 15 nm, corresponding to 0.11 eV, compared to that of the pure Liq film. Conversely, both the HOMO levels of Liq and the mixture of 50 wt% Liq and PVPh4Py were the same at 5.5 eV, as determined via by photoelectron yield spectroscopy. Consequently, the mixture of Liq and PVPh4Py had a smaller energy gap than that of Liq due to the lower LUMO level of the mixture than that of Liq (Figure 4b). Therefore, to understand the distribution of the HOMO and LUMO level in Liq, DFT calculations were conducted as shown in **Figure 5**. The HOMO is not located on the Li atom (Figure 5b), but the LUMO is associated with the Li atom (Figure 5c). These results suggest that the interactions between the Li atom of Liq and the pyridine ring of PVPh4Py affected the LUMO level. In addition, we also investigated UV absorption of the Liq solution using various solvents such as toluene, THF and pyridine, with concentration of 1×10^{-5} mol L^{-1} as shown in Figure S2 (Supporting Information). The pyridine solution exhibited red shift of absorption than those of the toluene and THF solution, indicating reduced energy gaps due to the interaction with pyridine.

2.3. Effect of the EIL Thickness and Liq Concentration on Device Performance

The performance of device with EILs of different thicknesses composed of the mixtures of PVPh4Py and Liq was investigated. The three types of EILs with thicknesses of 1.6, 8.6 and 16 nm were deposited from solutions with different Liq concentrations using different spin-coating speeds. **Figure 6**a,b show the dependence of the driving voltage and the EQE at 1000 cd m^{-2} on the thickness of EILs with different Liq concentrations. The devices with ultrathin (approximately 1.6 nm) EILs exhibited similar driving voltages and EQEs. As the EILs thickness was increased from 1.6 nm to 16 nm, the driving voltages increased and the EQEs decreased. However, the increase in the voltage and the decrease in the EQE were suppressed in the EILs composed of PVPh4Py and Liq compared to those for the

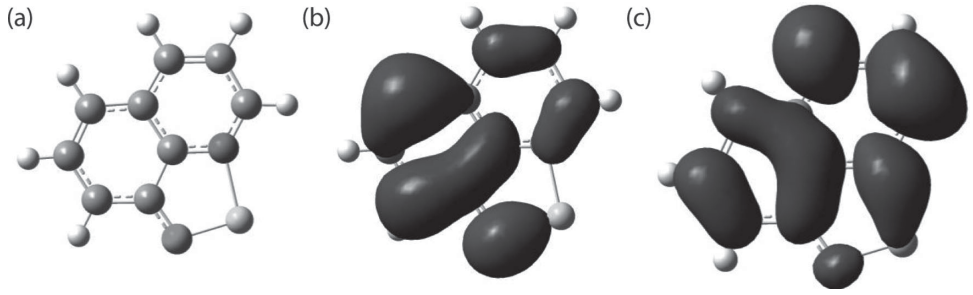

Figure 5. a) Molecular structure, b) HOMO, and c) LUMO of Liq with structures optimized in the ground states.

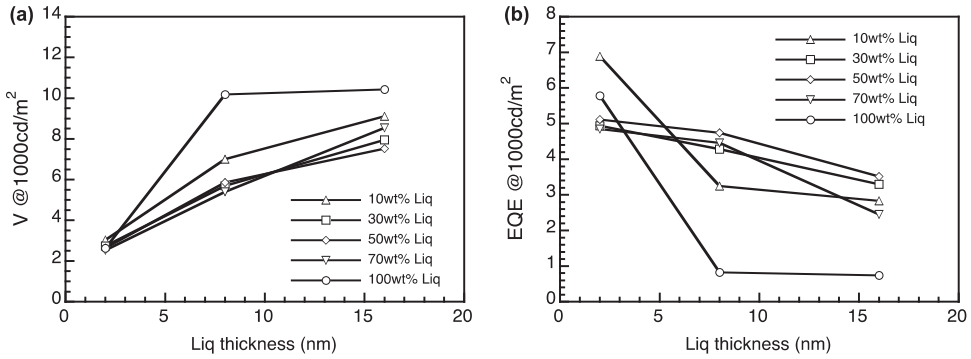

Figure 6. PLED performance as a function of the thickness of the PVPh4Py:Liq EILs: a) driving voltage and b) external quantum efficiency.

EIL composed of 100 wt% Liq. The device with a 50 wt% mixed EIL exhibited the least dependence on the layer thickness, and the lowest driving voltage and highest EQE for all of the devices was observed for an EIL with thickness of 16 nm. The high driving voltage and low efficiency of the device with the thick Liq layer is attributed to the poor electron transport properties of Liq itself. Conversely, mixing PVPh4Py with Liq could improve the electron transport properties of the EIL, and the driving voltage remained low, even for a thick EIL. The reduced dependence of EIL performance on the layer thickness will be advantageous for the large-area coating processes, because it is difficult using solution processing to form uniform thin films with an accuracy of a few nanometers.

2.4. Importance of the Position of the Pyridine Ring Substituent

Next, the influence of the position of the nitrogen in the pyridine rings was investigated using PVPh2Py, PVPh3Py, PVPh4Py, and PV4Py. Ultrathin (approximately 1.6 nm) and thin (approximately 8.6 nm) EILs composed of mixtures of the polymers and Liq were used, and the current density–voltage (*J*–*V*), luminance–voltage (*L*–*V*) characteristics and external quantum efficiency–current density (EQE–J) characteristics are shown in **Figure 7** and **Figure 8**, respectively. The devices with the ultrathin EILs exhibited similar turn-on voltages of 2.0 V and driving voltages of 2.2 V at 100 cd m^{-2}, respectively. The efficiencies were also similarly high at 1000 cd m^{-2}

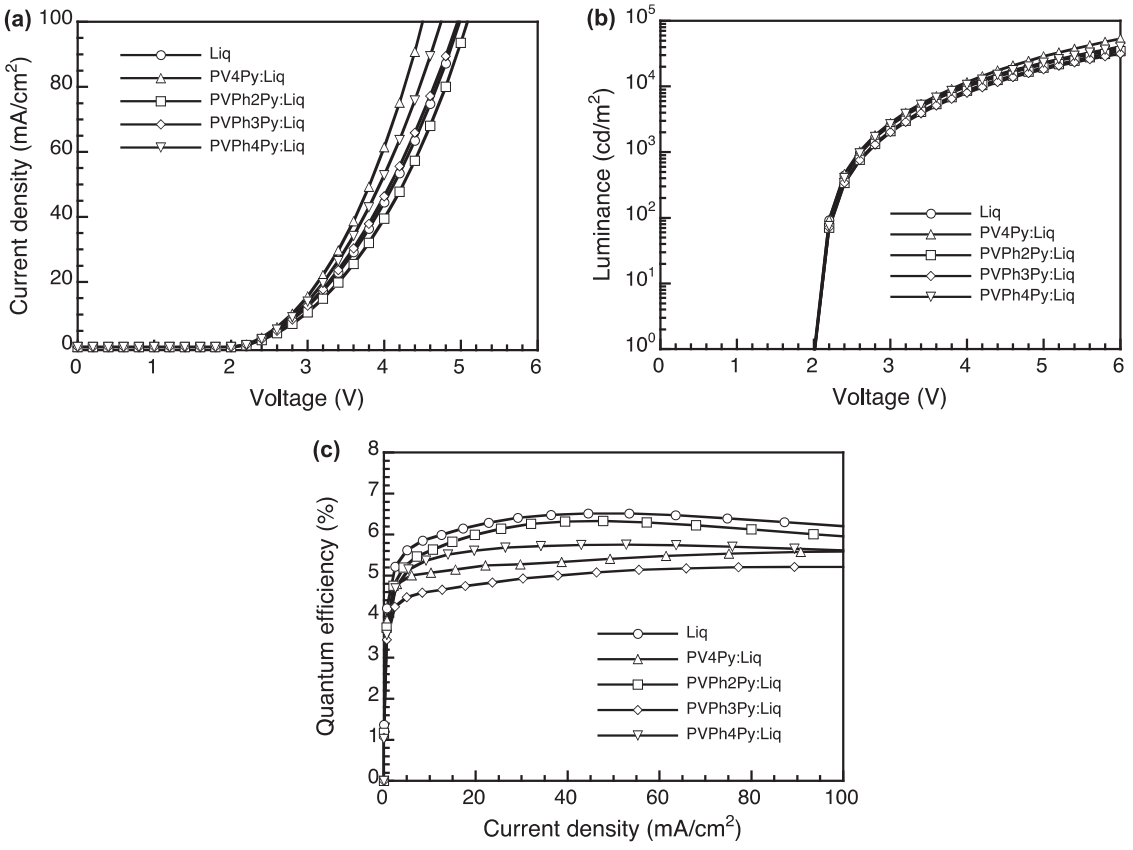

Figure 7. PLED performance with ultrathin EILs (1.6 nm) using PV4Py, PVPh2Py, PVPh3Py and PVPh4Py doped with 50 wt% Liq, respectively, and 100wt% Liq: a) current density–voltage characteristics, b) luminance–voltage characteristics, and c) external quantum efficiency–current density characteristics.

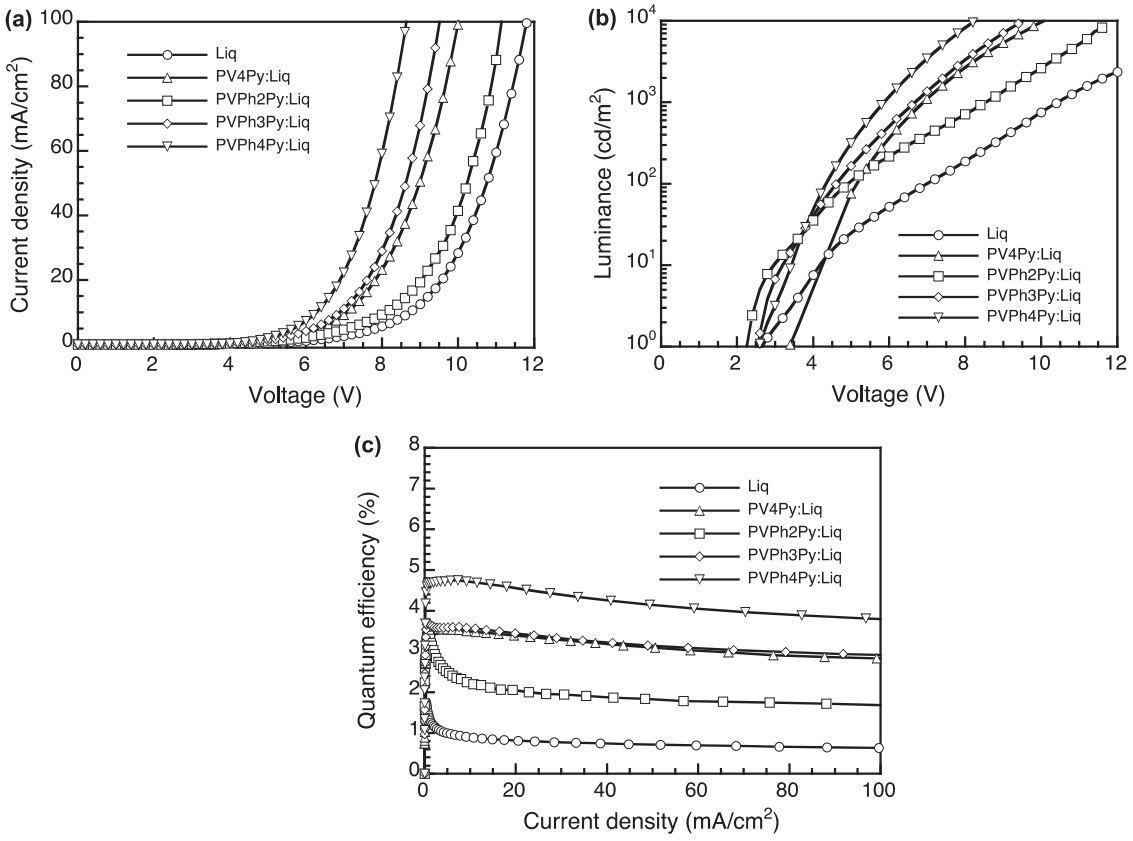

Figure 8. PLED performance with thin EILs (8.6 nm) using PV4Py, PVPh2Py, PVPh3Py and PVPh4Py doped with 50 wt% Liq, respectively, and 100w t% Liq: a) current density–voltage characteristics, b) luminance–voltage characteristics, and c) external quantum efficiency–current density characteristics.

(approximately 20 lm W^{-1} and 5% EQE). The position of the nitrogen in the pyridine rings had slight influence on the electron injection properties in the ultrathin layers (Figure 7). Conversely, in the devices with thin EILs (approximately 8.6 nm), the position of the nitrogen in the pyridine rings of the polymers had a greater influence on the driving voltage and efficiency. The driving voltage increased in the order of PVPh4Py < PVPh3Py < PVPh2Py (Figure 8a,b), and the device with an EIL composed of PVPh4Py:50 wt% Liq exhibited the lowest turn-on voltage and driving voltage of all of the polymers at 2.6 and 4.3 V, respectively at 100 cd m^{-2}, Alternatively, the EQE increased in the order PVPh2Py < PVPh3Py < PVPh4Py (Figure 8c). All of the device characteristics are summarized in Table S2 (Supporting Information). These results suggest that the position of the nitrogen in the pyridine rings significantly affects the electron transport properties of the polymers, rather than the electron injection properties. Sasabe et al. previously reported that the electron mobility of a series of oligo phenylpyridine derivatives were strongly affected by the position of the nitrogen in the pyridine rings due to C-H···N hydrogen bonding interactions.[29] In our case, similar interactions would explain the observed results. As mentioned in the discussion of the T_g, the intermolecular hydrogen bonding interaction of the nitrogen located at the four-positions of the PVPh4Py rings are stronger than those of the position of the nitrogen in the pyridine rings of PVPh3Py and PVPh2Py. The denser packing of PVPh4Py that results from the stronger hydrogen bonding interactions probably leads to the enhanced electron transport properties observed for the thick films.

3. Conclusion

A series of (vinylphenyl)pyridine-based polymer binders, PVPh2Py, PVPh3Py, and PVPh4Py, were designed and synthesized. Mixtures of Liq and the polymers exhibited superior electron injection characteristics as ultrathin (1.6 nm) EIL films that were comparable to those of EILs composed only of Liq. Thus, the addition of the polymers did not deteriorate the performance of Liq EILs. In addition, as increasing the EIL thickness increased from 1.6 nm to 16 nm, the driving voltages increased and the EQEs decreased. However, the increase in the voltage and decrease in the EQE were suppressed in the device with mixed EILs compared to those observed for the device with composed of 100 wt% Liq. In the thin layers, the driving voltage increased in the order of PVPh4Py < PVPh3Py < PVPh2Py. Furthermore, the position of the nitrogen in the pyridine ring is considered to affect the electron transport properties of the EILs. The mixing PVPh4Py with Liq improved the driving voltage of the fabricated devices, even with a thick mixed EIL. This reduced dependence of the performance of EILs on their thickness will be advantageous for coating of large areas using solution processes.

4. Experimental Section

Synthesis of ***1***: 2-bromopyridine (1.95 g, 12.3 mmol) and 4-vinylphenylboronic acid (1.27 g, 8.58 mmol) were added to a round-bottom flask. Tetrahydrofuran (12.5 mL) and aqueous potassium carbonate (2 M, 6.33 mL) were added and nitrogen bubbling through the mixture for 30 min. Then, tetrakis(triphenylphosphine)palladium (0) (7.9 mg, 6.8 μmol) was added and the resultant mixture was stirred for 20 h at 66 °C under N_2 flow. The resulting mixture was cooled to room temperature, and then dichloromethane was added. The organic layer was washed with water, dried over magnesium sulfate and filtered. The solvent was moved in vacuo, and the residue was purified by column chromatography over silica using an ethyl acetate-hexane mixture (1:4) as eluent to give **1** (832 mg, 53%):^{1}H-NMR (400 MHz $CDCl_3$), 8.67–8.65 (dt, 1 H, J = 4.4 Hz, 2.8 Hz), 8.35–8.33 (dd, 1 H, J = 4.4 Hz, 1.6 Hz), 7.96–7.93 (dt, 1 H, J = 8.8 Hz, 4.0 Hz), 7.70–7.68 (m, 1 H), 7.51–7.34 (m, 4 H), 6.77–6.70 (dd, 1 H, J = 18 Hz, 11 Hz), 5.82–5.78 (d, 1 H, J = 18 Hz), 5.29–5.26 (d, 1 H, J = 11 Hz).

Synthesis of ***2***: 3-bromopyridine (1.95 g, 12.3 mmol) and 4-vinylphenylboronic acid (1.27 g, 8.58 mmol) were added to a round-bottom flask. Tetrahydrofuran (12.5 mL) and aqueous potassium carbonate (2 M, 6.33 mL) were added and nitrogen bubbling through the mixture for 30 min. Then, tetrakis(triohenylphosphine)palladium (0) (7.9 mg, 6.8 μmol) was added and the resultant mixture was stirred for 20 h at 66 °C under N_2 flow. The resulting mixture was cooled to room temperature, and then dichloromethane was added. The organic layer was washed with water, dried over magnesium sulfate and filtered. The solvent was moved in vacuo, and the residue was purified by column chromatography over silica using an ethyl acetate-hexane mixture (2:3) as eluent to give 1 (724 mg, 47%): ^{1}H-NMR (400 MHz $CDCl_3$), 8.86 (d, 1 H, J = 2.4 Hz), 8.59–8.57 (dd, 1 H, J = 5.2 Hz, 1.6 Hz), 7.89–7.86 (dt, 1 H, J = 8.0 Hz, 3.6 Hz), 7.57–7.51 (m, 4 H), 7.38–7.34 (dd 1 H, J = 8.0 Hz, 5.0 Hz), 6.79–6.72 (dd, 1 H, J = 18 Hz, 11 Hz), 5.84–5.80 (d, 1 H, J = 18 Hz), 5.32–5.29 (d, 1 H, J = 11 Hz).

Synthesis of ***3***: 4-bromopyridine hydrochloride (1.95 g, 10.0 mmol) and 4-vinylphenylboronic acid (1.27 g, 8.58 mmol) were added to a round-bottom flask. Tetrahydrofuran (50.0 mL) and aqueous potassium carbonate (3.58 M, 6.33 mL) were added and nitrogen bubbling through the mixture for 30 min. Then, tetrakis(triohenylphosphine)palladium (0) (7.9 mg, 6.8 μmol) was added and the resultant mixture was stirred for 20 h at 66 °C under N_2 flow. The resulting mixture was cooled to room temperature, and then dichloromethane was added. The organic layer was washed with water, dried over magnesium sulfate and filtered. The solvent was moved in vacuo, and the residue was purified by column chromatography over silica using an ethyl acetate-hexane mixture (3:2) as eluent to give 1 (790 mg, 51%): ^{1}H-NMR (400 MHz $CDCl_3$), 8.65 (d, 1 H, J = 6.0 Hz), 7.61 (d, 1 H, J = 8.0 Hz), 7.53–7.49 (m, 4 H), 6.80–6.72 (dd, 1 H, J = 18 Hz,11 Hz), 5.83 (d 1 H, J = 18 Hz), 5.33 (d, 1 H, J = 11 Hz).

Polymerization: Anhydrous tetrahydrofuran (1.0 mL), benzoylperoxide (4.0 mg, 16.5 μmol) and (vinylphenyl)pyridine monomer (400 mg, 2.21 mmol for 1 400 mg, 2.21 mmol for 2 and 0.40 g, 2.21 mmol for 3) were stirred for 48 h at 80 °C under vacuum. The solvent was moved in vacuo, and the residue was purified by reprecipitation using a hexane as eluent to give PVPh2Py (80 mg, 20%), PVPh3Py (50 mg, 13%) and PVPh4Py (250 mg, 68%).

Device Fabrication: All PLEDs were grown on glass substrates pre-coated with indium tin oxide (ITO) with sheet resistance of 15 Ω sq^{-1}. These ITO substrates were cleaned ultrasonically with deionized water and 2-propanol, followed by a UV-ozone treatment for 20 min. PEDOT:PSS solution in water (CLEVIOS CH8000) was filtered through a syringe filter (0.45 μm) to remove any large particles, then spin-coated onto ITO substrate and annealed at 200 °C for 10 min in an ambient condition with a thickness of 30 nm. TFB (from American Dye Source) was spin coated from a *p*-xylene solution with a concentration of 7 mg mL^{-1} onto PEDOT:PSS and annealed at 180 °C for 60 min in an nitrogen filled condition to obtain a insoluble film to typical organic solvents with a thickness of 20 nm. F8BT (from Sumitomo Chemical) was spin coated from *p*-xylene solution with a concentration of 12 mg mL^{-1} onto TFB and annealed at 130 °C for 10 min in a nitrogen filled condition with a thickness of 80 nm. For fabrication of electron injection layer with Liq and vinyl polymers were dissolved in 2-ethoxyethnol with concentration of 1 mg mL^{-1} for ultrathin layer (ca. 1.6 nm) and 3 mg mL^{-1} for thin layer (ca. 8.6 nm) and thick layer (ca. 16 nm) using a different spin speed, respectively, then blending the Liq and vinyl polymers solution in a 1:1 volume ratio with Liq doping concentration of 50 wt%. These solutions were spin coated onto F8BT layer. As a cathode, Al was deposited by thermal evaporated under high vacuum (≈10^{-5} Pa). The PLEDs were encapsulated using an epoxy glue and glass cover, before the characterizations.

Characterization: ^{1}H NMR spectra were obtained in a JEOL 400 (400 MHz) spectrometer. Molecular weight of vinyl polymer were measured by a gel permeation chromatography (HITACHI L-7000). Differential scanning calorimetry was performed using a Perkin-Elmer Diamond DSC Pyris instrument under nitrogen atmosphere at a heating rate of 10 °C min^{-1}. Thermogravimetric analysis was undertaken using a SEIKO EXSTAR 6000 TG/DTA 6200 unit under nitrogen atmosphere at a heating rate of 10 °C min^{-1}. HOMO level were determined by photoelectron yield spectroscopy (Sumitomo Heavy Industries PYS). UV–vis spectra were measured using a Shimadzu UV-3150. Film thickness were measured by X-ray refraction with SmartLab or by a dektak 8. Electroluminescence (EL) spectra were measured using a Hamamatsu PMA-11 photonic multichannel analyzer. The current density–voltage and luminance–voltage characteristics were measured using a Keithley source measure unit 2400 and a Minolta CS200 luminance-meter, respectively. External quantum efficiencies were calculated from the front luminance, current density, and EL spectrum.

Supporting Information

Supporting Information is available from the Wiley Online Library or from the author.

Acknowledgements

The authors would like to thank the "Strategic Promotion of Innovative R&D Program" and "Japan Regional Innovation Strategy Program by Excellence" of Japan Science and Technology Agency (JST) for financial support, and Sumitomo chemical for material support.

Received: April 3, 2014
Revised: May 7, 2014
Published online: July 17, 2014

[1] R. H. Friend, R. W. Gymer, A. B. Holmes, J. H. Burroughes, R. N. Marks, C. Taliani, D. D. C. Bradley, D. A. Dos Santos, J. L. Bredas, M. Logdlund, W. R. Salaneck, *Nature* **1999**, *397*, 121.
[2] P. K. H. Ho, J. S. Kim, J. H. Burroughes, H. Becker, S. F. Y. Li, T. M. Brown, F. Cacialli, R. H. Friend, *Nature* **2000**, *404*, 481.
[3] B. H. Zhang, G. P. Tan, C. S. Lam, B. Yao, C. L. Ho, L. H. Liu, Z. Y. Xie, W. Y. Wong, J. Q. Ding, L. X. Wang, *Adv. Mater.* **2012**, *24*, 1873.
[4] G. Liaptsis, K. Meerholz, *Adv. Funct. Mater.* **2013**, *23*, 359.
[5] X. Gong, W. L. Ma, J. C. Ostrowski, G. C. Bazan, D. Moses, A. J. Heeger, *Adv. Mater.* **2004**, *16*, 615.
[6] J.-S. Kim, R. H. Friend, I. Grizzi, J. H. Burroughes, *Appl. Phys. Lett.* **2005**, *87*, 023506.
[7] H. B. Wu, J. H. Zou, F. Liu, L. Wang, A. Mikhailovsky, G. C. Bazan, W. Yang, Y. Cao, *Adv. Mater.* **2008**, *20*, 696.
[8] X. Gong, S. Wang, D. Moses, G. C. Bazan, A. J. Heeger, *Adv. Mater* **2005**, *17*, 2053.

[9] S. Sax, N. Rugen-Penkalla, A. Neuhold, S. Schuh, E. Zojer, E. J. List, K. Mullen, *Adv. Mater.* **2010**, *22*, 2087.
[10] T. Earmme, E. Ahmed, S. A. Jenekhe, *Adv. Mater.* **2010**, *22*, 4744.
[11] T. Ye, S. Shao, J. Chen, L. Wang, D. Ma, *ACS Appl. Mater. Interfaces* **2011**, *3*, 410.
[12] T. W. Lee, O. O. Park, L. M. Do, T. Y. Zyung, T. Ahn, H. K. Shim, *J. Appl. Phys.* **2001**, *90*, 2128.
[13] T. W. Lee, O. O. Park, *Adv. Mater.* **2001**, *13*, 1274.
[14] H. B. Wu, F. Huang, Y. Q. Mo, W. Yang, D. L. Wang, J. B. Peng, Y. Cao, *Adv. Mater.* **2004**, *16*, 1826.
[15] C. V. Hoven, A. Garcia, G. C. Bazan, T.-Q. Nguyen, *Adv. Mater.* **2008**, *20*, 3793.
[16] F. Huang, Y. Zhang, M. S. Liu, A. K. Y. Jen, *Adv. Funct. Mater.* **2009**, *19*, 2457.
[17] X. Guan, K. Zhang, F. Huang, G. C. Bazan, Y. Cao, *Adv. Funct. Mater.* **2012**, *22*, 2846.
[18] Y. Zhou, C. Fuentes-Hernandez, J. Shim, J. Meyer, A. J. Giordano, H. Li, P. Winget, T. Papadopoulos, H. Cheun, J. Kim, M. Fenoll, A. Dindar, W. Haske, E. Najafabadi, T. M. Khan, H. Sojoudi, S. Barlow, S. Graham, J. L. Bredas, S. R. Marder, A. Kahn, B. Kippelen, *Science* **2012**, *336*, 327.
[19] G. E. Lim, Y. E. Ha, M. Y. Jo, J. Park, Y. C. Kang, J. H. Kim, *ACS Appl. Mater. Interfaces* **2013**, *5*, 6508.
[20] C. Min, C. Shi, W. Zhang, T. Jiu, J. Chen, D. Ma, J. Fang, *Angew. Chem. Int. Ed.* **2013**, *52*, 3417.
[21] L. S. Hung, C. W. Tang, M. G. Mason, *Appl. Phys. Lett.* **1997**, *70*, 152.
[22] J. Lee, Y. Park, D. Y. Kim, H. Y. Chu, H. Lee, L. M. Do, *Appl. Phys. Lett.* **2003**, *82*, 173.
[23] J. Huang, T. Watanabe, K. Ueno, Y. Yang, *Adv. Mater.* **2007**, *19*, 739.
[24] J. Huang, Z. Xu, Y. Yang, *Adv. Funct. Mater.* **2007**, *17*, 1966.
[25] T. Chiba, Y.-J. Pu, H. Sasabe, J. Kido, Y. Yang, *J. Mater. Chem.* **2012**, *22*, 22769.
[26] G. A. H. Wetzelaer, A. Najafi, R. J. P. Kist, M. Kuik, P. W. M. Blom, *Appl. Phys. Lett.* **2013**, *102*, 053301.
[27] T. Chiba, Y. J. Pu, M. Hirasawa, A. Masuhara, H. Sasabe, J. Kido, *ACS Appl. Mater. Interfaces* **2012**, *4*, 6104.
[28] L. P. Lu, D. Kabra, R. H. Friend, *Adv. Funct. Mater.* **2012**, *22*, 4165.
[29] H. Sasabe, D. Tanaka, D. Yokoyama, T. Chiba, Y.-J. Pu, K. Nakayama, M. Yokoyama, J. Kido, *Adv. Funct. Mater.* **2011**, *21*, 336.